International Journal of Multidisciplinary Science and Innovation (IJMSI)
International Conference on Advances in Physical, Chemical and Mathematical Sciences for Sustainable Development
Organized by
D.M.S. Mandal's Bhaurao Kakatkar College, Belgaum, Karnataka, India
Website: https://ijmsi.in/
ISSN: 3107-5754 I Vol. 2, Special Issue 1, 2026 I Page No.: 21-30

Research

Modifying the Structural, Morphological and Dielectric Properties of ZnO Nanoparticles via Co and Ni Doping

Preeti Patil[1,2*], Shivshankar G.[1], Bhimraya Biradar[1], Basavaraja Sannakki[2*] and Shridhar Mathad[3]

[1]*Department of Physics, Government First Grade College Haliyal,*
[2]*Department of Physics, Gulbarga University, Kalaburgi, India*
[3]*Department of Physics, K.L.E. Institute of Technology, Gokul, Hubballi, India.*

Corresponding Author:
Preeti Patil

Email:
preetigfgch23@gmail.com, sannakki@rediffmail.com

DOI: *10.62896/ijmsi.2.s1.03*

Conflict of interest: *NIL*

Article History
Received: 08/06/2026
Accepted: 16/06/2026
Published: 20/06/2026

Abstract:
Pure ZnO and (TM) transition metal-doped ZnO NPs ($M_XZn_{1-X}O$ NPs M=Co and Ni with X= 0%, 15%, 25%, 35% and 45%) were prepared by using Sol-gel autocombustion method using metal nitrate precursor and sucrose (bio fuel) followed by annealing at 800°C. The synthesized pure ZnO and doped ZnO nanoparticles were evaluated using X-ray diffraction analysis (XRD) and scanning electron microscopy (SEM). The XRD data revealed that the samples exhibited crystalline characteristics with a hexagonal wurtzite structure. Structural parameters, including lattice constants (a and c), the crystallite sizes (D), volume of the unit cell (V) and microstrain (ε) were determined. SEM results showed more porous and loosely agglomerated nanostructures with increased doping. Compared to Ni^{2+} or pure ZnO, Co^{2+} exhibits a greater spike in polarization, dielectric response and conductivity because of its stronger d-orbital interactions. Furthermore, Co and Ni doped ZnO exhibit a higher dielectric loss compared to pure ZnO.

Keywords: ZnO, Sol-Gel auto-combustion, XRD, SEM, Dielectric loss.

1. Introduction

In the last few years, wide band gap metal semiconductor oxide materials have gained lot of interest because of the rapid advancement of diluted magnetic semiconductors (DMSs), which exhibit distinctive magnetic and electrical properties. Zinc oxide (ZnO) is one of the most favoured materials due to its wide band gap (~3.37 eV), natural abundance, ease of fabrication, and high chemical stability [1,2]. ZnO exhibits desirable properties including semiconducting behavior, piezoelectricity, chemical sensing capability, and good electrical conductivity. Furthermore, doping ZnO with transition metals (TMs) produces defects which leads to notable changes in its crystal structure that affects its characteristics and ultimately its potential uses. Research has shown that ZnO doped with transition metals exhibit good semiconducting response and high soluability [3]. Several researchers have explored that doping ZnO with specific TM dopants such as Ni^{2+} [4], Ag^{2+} [5], Mn^{2+} [5], Co^{2+} [7], and Al^{3+} [8] has been demonstrated to be a successful approach for enhancing the optical, dielectric and magnetic behavior of ZnO.

Co and Ni-doped ZnO NPs stand out as highly promising candidates owing to their distinctive properties, including chemical stability, cost effectiveness, high efficiency, non-toxicity, and environmental friendliness. Several investigations have examined ZnO modified with Co and Ni dopants, that produce charge carriers when exposed to visible light. However, Co- and Ni-doped ZnO variants prove particularly advantageous due to their excellent catalytic activity in oxygen reduction, elevated electrical conductivity, and superior chemical stability. As a result, these materials demonstrate remarkable dielectric properties, with enormous dielectric constants and small dielectric loss, making them strong contenders for dielectric components in

photodetectors. Overall, the elevated dielectric constant stems from extrinsic effects [9,10]. Dopant-induced defects in these metal oxides alter donor densities and band structures, thereby tuning optical and electronic properties. While ZnO hosts various defects, oxygen vacancies remain the most dominant. Theoretical and experimental investigations reveal that oxygen vacancies dictate electronic structure, surface properties and charge transport in ZnO. Generally, oxygen vacancies create isolated shallow donor levels within the bandgap, enhancing charge generation and separation. Additionally, they act as active sites for surface adsorption and desorption. Hence, significant research has pursued controlled synthesis of Co- and Ni-doped ZnO nanoparticles with tailored oxygen vacancy concentrations to leverage their outstanding electrical and dielectric performance in UV photodetectors.

Muhammad A. et al. (2023) found that the dielectric constant of Co-doped ZnO nanoparticles enhanced with increasing Co content, while dielectric loss decreased, indicating improved dielectric behavior. Additionally, the AC conductivity rose with frequency, suggesting enhanced electrical performance and making these nanoparticles suitable for low-frequency optoelectronic and spintronic applications.[11] Senthilkumar N. et al. (2024) inquired the pure and Co–Ni co-doped ZnO nanorods synthesized via co-precipitation method. It is observed that increasing dopant concentration led to larger crystallite size, reduced defects and stress, a narrower band gap, and wider nanorods. The co-doped nanorods also showed improved electrical conductivity and dielectric properties, making them promising for optoelectronic applications [12]. Paskaleva, A et al. (2024) showed that Ni and Fe doped ZnO enabled tunable physical and potential magnetic properties, prepared by atomic layer deposition (ALD) providing precise control over thin film composition and structure. The study shows that dopants significantly influence the electrical, dielectric, and optical behavior of ZnO films, with different polarization mechanisms governing the dielectric response. These results demonstrated how dopant type can be used to customize ZnO thin films for cutting edge uses [13]. Athira A et al. (2025) synthesized Mg- and Ni-doped as well as co-doped ZnO using a straightforward and affordable precipitation method with different dopant concentrations. Structural, optical, and compositional analyses confirmed successful modification of ZnO, along with changes in band gap energy. The doped and co-doped samples also showed notable variations in electrical and dielectric properties, highlighting the benefits of co-doping [14]

ZnO nanoparticles have been synthesized using a range of physical and chemical methods including including, sol-gel method [15], hydrothermal method [16], mechanical alloying techniques [17], physical vapor deposition (PVD), chemical vapor deposition (CVD)[18,19], laser ablation, plasma synthesis techniques [20] and spray coating [21,22]. Among these procedures, the sol–gel method is considered the most efficient for producing metal oxide nanopowders due to its simplicity, cost-effectiveness, rapid processing, and low-temperature requirements [23]. The majority of these methods look for an extra calcination step to improve the crystallinity of the resulting nanoparticles [24-26].

In this research investigation, we synthesized high-quality $Co_xZn_{1-x}O$ and $Ni_xZn_{1-x}O$ (where x = 0.00 to 0.45) nanoparticles with controlled and fairly uniform size using the sol-gel auto-combustion method. The impact of Co/Ni doping on the structural, morphological and dielectric characteristics of ZnO was investigated using the synthesized nanoparticles.

2. Experimental Methods.

2.1 Materials

Sigma-Aldrich provided highly pure (99.99%) chemical reagents like Zinc nitrate hexahydrate ($Zn(NO_3)_2.6H_2O$), Cobaltous nitrate hexahydrate ($CO(NO_3)_2.6H_2O$), Nickel nitrate hexahydrate ($Ni(NO_3)_2.6H_2O$), Sucrose($C_{12}H_{22}O_{11}$), Polyvinyl Alcohol($C_2H_4O)_n$ and double distilled water(DW) were used

2.2 Synthesis of pure ZnO and Co/Ni doped ZnO Nanoparticles.

Pure ZnO nanoparticles were produced by dissolving 10 g of zinc nitrate hexahydrate in 50 mL of DW, followed by the addition of 30 g of sucrose dissolved in another 50 mL of DW. Subsequently, 10 cc of PVA solution was introduced, then the mixture was magnetically agitated at 80°C for 90 minutes to achieve homogeneity. The resulting solution was heated in a glass beaker over a medium flame for about 3 hours until auto-combustion occurred, producing a black powder, which was then cooled down to room temperature and ground using an agate mortar. The obtained nanopowder was annealed at 800°C for 8 hours to eliminate impurities and improve crystallinity. Cobaltous nitrate hexahydrate and Nickel nitrate hexahydrate were added separately to the

International Journal of Multidisciplinary Science and Innovation (IJMSI)
International Conference on Advances in Physical, Chemical and Mathematical Sciences for Sustainable Development
Organized by
D.M.S. Mandal's Bhaurao Kakatkar College, Belgaum, Karnataka, India
Website: https://ijmsi.in/
ISSN: 3107-5754 I Vol. 2, Special Issue 1, 2026 I Page No.: 21-30

precursor solution in stoichiometric ratios of 15%, 25%, 35%, and 45% in order to produce cobalt doped and Nickel doped ZnO samples.

2.3 Characterization Techniques

The XRD study of prepared pure ZnO, Co/Ni-doped ZnO NPs (15%, 25%, 35% and 45%) were examined at room temperature using X-ray powder Diffraction (Rigaku Smartlab SE) with Cu Kα (1.5406 Å) radiation and 10º/min operating rate at 40kV/30Ma and scanning angle range 2θ between 20º-80º. A scanning electron microscope (SEM) (Model: JSM-IT500) was used to study the morphology of the synthesized nanoparticles. The dielectric constant (ε_r), dielectric loss (tanδ) and AC conductivity (σ_{ac}) of the synthesized NPs were studied at room temperature using Hioki IM3570 impedance analyzer. Measurements were conducted at room temperature between 4Hz and 1MHz frequency band.

3. **Results and Discussions**

3.1 Structural studies

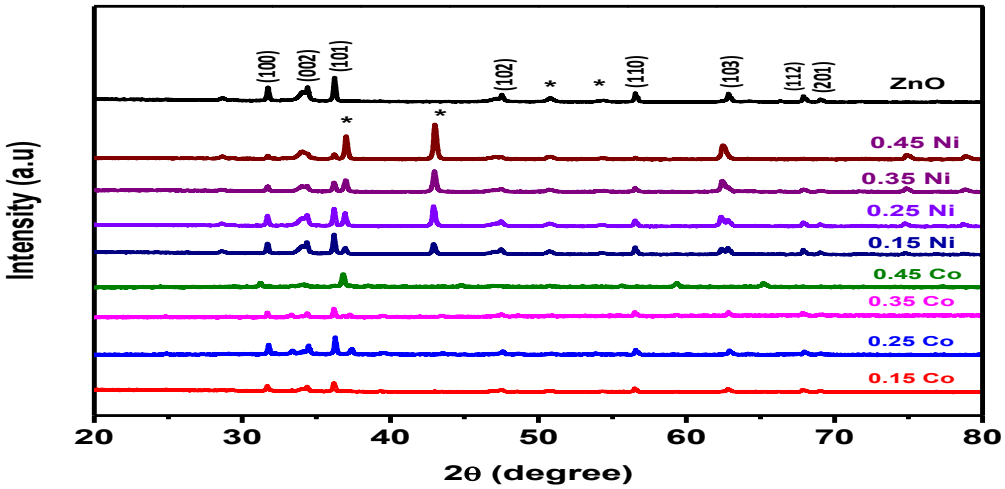

Fig. 1 X-ray diffraction patterns of ZnO and Co/Ni doped ZnO nanoparticles.

The XRD patterns of pure, Co/Ni-doped ZnO NPs confirm that all samples predominantly retain the hexagonal structure with wurtzite phase in good confirmity with JCPDS standards (No. 36-1451), indicating successful integration of Co^{2+} and Ni^{2+} ions into the lattice of ZnO l [27-28]. In fig 1.the prominent peak reflections observed at 31.7°, 34.4°, 36.2°, 47.5°, 56.5°, 62.9°, 67.9°, and 69.0° relates to the (100), (002), (101), (102), (110), (103), (112), and (201) planes, respectively. In both Ni- and Co-doped ZnO, slight shifts in peak positions toward higher 2θ values are observed with increasing dopant concentration, which can be due to lattice strain caused by the addition of smaller Ni^{2+} (0.69 Å) and Co^{2+} ions for that of Zn^{2+} (0.74 Å), leading to reduced lattice parameters. A gradual decrease in peak intensity along with peak broadening indicates reduced crystallinity and increased lattice disorder due to defect formation. For Ni-doped ZnO, crystallite size initially decreases at lower concentrations due to grain growth suppression by lattice strain, but increases at higher doping levels as a result of dopant saturation and particle coalescence. Additionally, the occurance of secondary peaks around 36.98° and 42.97° at higher Ni concentrations confirms the formation of a zinc nickel oxide phase (JCPDS 80-0075), particularly beyond 6% molar doping [29]. In contrast, Co-doped ZnO does not show any secondary phases, suggesting homogeneous incorporation of Co^{2+} within the lattice. The crystallite size in Co-doped samples exhibits a non-linear variation with doping concentration, reflecting competing effects of strain and growth kinetics. Debye–Scherrer equation was employed to calculate the average crystallite size which

$$D = K\lambda/\beta\cos\theta$$

falls within the nanometre range for all samples, confirming their nanoscale nature. Overall, both Ni and Co doping induce significant structural modifications, including crystallite size variation, lattice distortion and defect generation which strongly influence the structural properties of ZnO nanoparticles. A comprehensive structural detail has been presented in Table.No.1.

Compounds	Average Crystallite Size(nm)	Average Lattice Strain (ε)	d_{101}(Å)	Lattice parameters (Å)		c/a
				a	c	
ZnO	67	0.0013	2.478	3.252	5.205	1.600
$Co_{0.15}Zn_{0.85}O$	57	0.0019	2.480	3.255	5.206	1.599
$Co_{0.25}Zn_{0.75}O$	68	0.0014	2.475	3.249	5.199	1.599
$Co_{0.35}Zn_{0.65}O$	78	0.0013	2.480	3.255	5.205	1.599
$Co_{0.45}Zn_{0.55}O$	37	0.0046	2.44	3.221	5.362	1.664
$Ni_{0.15}Zn_{0.85}O$	68	0.0012	2.480	3.254	5.211	1.602
$Ni_{0.25}Zn_{0.75}O$	54	0.0016	2.480	3.255	5.207	1.600
$Ni_{0.35}Zn_{0.65}O$	49	0.0026	2.481	3.254	5.208	1.600
$Ni_{0.45}Zn_{0.55}O$	81	0.0013	2.480	3.260	5.107	1.566

Table 1. XRD calculations for pure ZnO and Co/Ni-doped ZnO nanoparticles

3.2 Morphological Studies

As shown in fig. 2. SEM images of synthesized undoped ZnO and Co/Ni-doped ZnO samples (15%, 25%, 35%, and 45%) reveal significant morphology-dependent changes with dopant concentration.

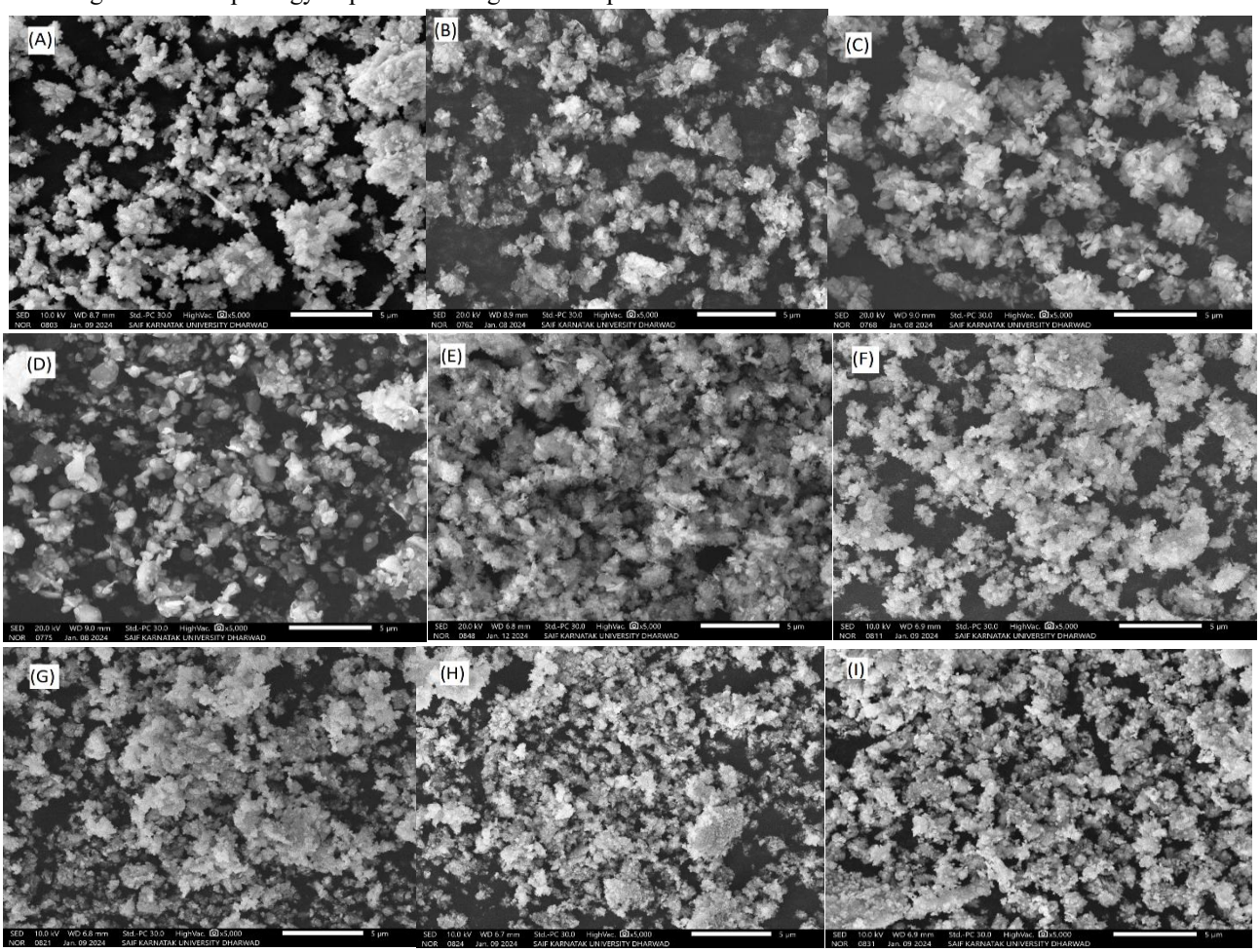

Fig 2. SEM images of (A) Pure ZnO, (B) $Co_{0.15}Zn_{0.85}O$, (C) $Co_{0.25}Zn_{0.75}O$, (D)$Co_{0.35}Zn_{0.65}O$, (E) $Co_{0.45}Zn_{0.55}O$ (F) $Ni_{0.15}Zn_{0.85}O$, (G) $Ni_{0.25}Zn_{0.75}O$, (H) $Ni_{0.35}Zn_{0.65}O$ and (H) $Ni_{0.45}Zn_{0.55}O$

Pure ZnO exhibits relatively uniform, quasi-spherical particles with slight agglomeration due to high surface energy. Co-doping increases agglomeration progressively, with intermediate concentrations promoting grain growth and higher concentrations leading to dense, compact structures with reduced porosity. This indicates that Co enhances grain coalescence through lattice distortion and diffusion effects.

In contrast, Ni doping initially produces finer and better-dispersed particles at low concentration. However, with increasing Ni content, clustering and eventual agglomeration occur, though generally less dense than in Co-doped samples. Overall, Ni reduces particle size at lower levels but leads to aggregation at higher concentrations due to increased defect density and surface energy. Such morphological modifications enhance the specific surface area and inter-particle connectivity, which is advantageous for applications like photocatalysis and sensing because of the presence of more active sites. These observations are consistent with XRD results, which show increased disorder and peak broadening at higher dopant concentrations, confirming the impact of Co and Ni doping on the morphological and structural characteristics of ZnO NPs.

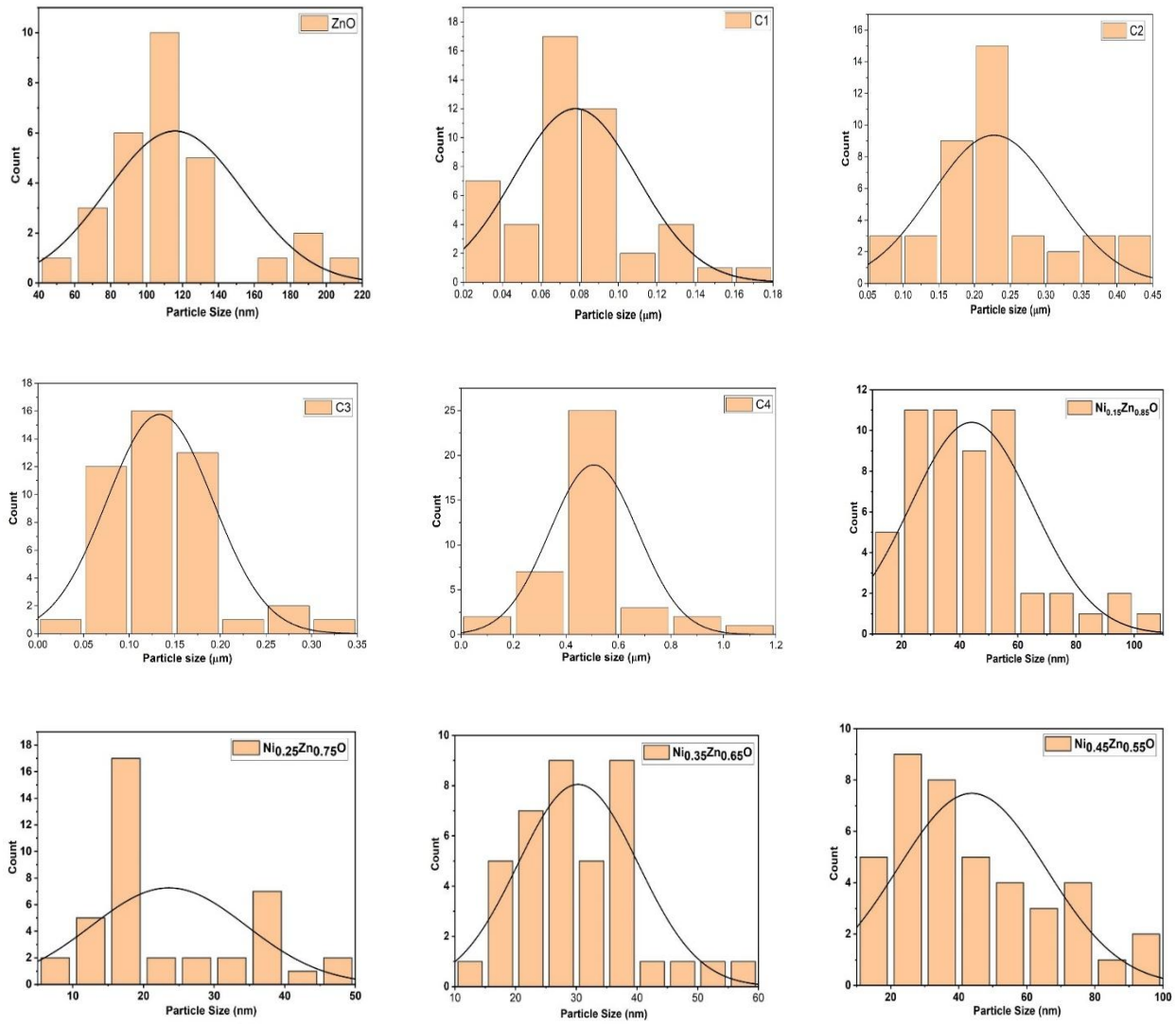

Fig. 3 Histogram of Particle size distribution of ZnO and Co/Ni-doped ZnO NPs.

The histograms showing particle size distribution of prestine ZnO and Co/Ni-doped ZnO NPs, derived from SEM micrographs using Image J software, are presented in Fig. 3. These histograms clearly demonstrate that Co/Ni doping produces a profound effect on the morphology of ZnO NPs. Pure ZnO shows a wide, polydisperse size distribution with a peak around 100–120 nm, indicating pronounced agglomeration and non-uniform growth. As Co doping increases from 15% to 45% the peak frequency ranges between 75-85nm, 220-230 nm, 125-135 nm and 495-505 nm respectively. With the introduction of Ni, the distribution shifts toward smaller particle sizes with better uniformity, suggesting that Ni ions suppress grain growth. With increase in the concentration of Ni doping from 15% to 45%, the peak frequency ranges are observed at 35–50 nm, 15–25 nm, 30–40 nm, and 40–55 nm, respectively. However, excessive Ni doping leads to a broader size distribution and increased agglomeration, resulting in reduced uniformity, which is in strong agreement with the XRD findings.

3.3 Dielectric measurements

3.3.1 Frequency-Dependent Dielectric Constant (ε′)

The dielectric constant (ε′) of undoped ZnO and Ni/Co-doped ZnO samples shows typical dispersive behavior, with high ε′ values at lower frequencies followed by a sharp decline and saturation at high frequencies as in fig.4. The Maxwell-Wagner polarization mechanism provides a clear explaination of this behavior, which arises from the inhomogeneity of polycrystalline ZnO, consisting of semiconducting grains divided by insulating grain boundaries. Charge carriers bulid up at these interfaces at low frequencies, increasing space charge polarization and raising dielectric constant values. With increasing frequency, the polarization mechanism is unable to follow the rapidly fluctuating electric field, which decreases ε′. This dispersion is further supported by Koop's phenomenological theory, which describes the dielectric response as a combination of highly resistive and conductive grains.

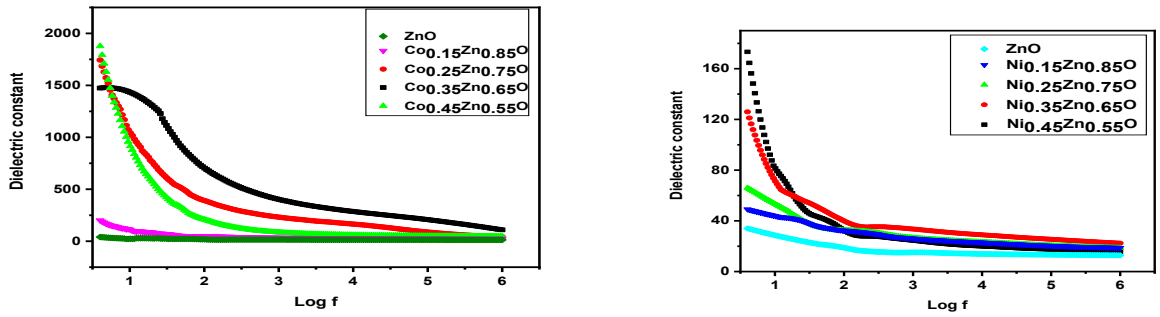

Fig.4. Dielectric constant and frequency variation of ZnO, Co /Ni doped ZnO NPs.

Doping ZnO with transition metal ions like Ni^{2+} and Co^{2+} creates localized states within the band structure, altering the dielectric response. The incorporation of Ni^{2+} ions causes lattice distortion and increased defect states, promoting charge carrier hopping and polarization. Co^{2+} ions have stronger electronic interactions with partially filled d-orbitals, leading to increased polarization and dielectric response compared to pure ZnO.

3.3.2 Dielectric loss

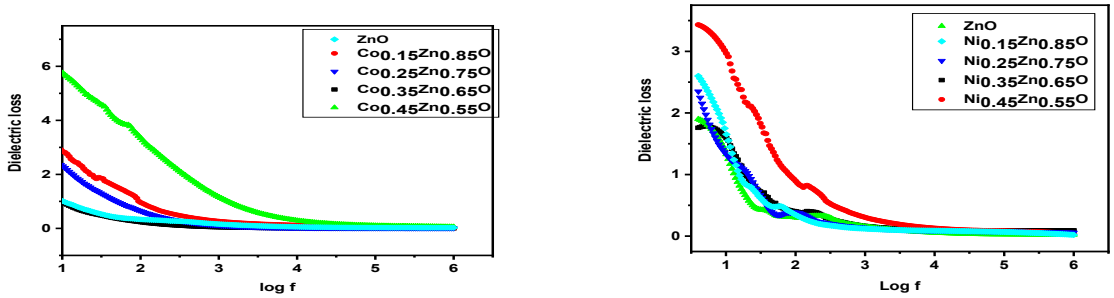

Fig.5 Dielectric loss versus frequency of Pure ZnO, Co/Ni-doped ZnO nanoparticles.

The dielectric loss (tan δ) of ZnO and Co/Ni-doped ZnO samples decreases with increasing frequency, as expected for semiconducting oxide materials(fig.5). Lower frequencies show larger dielectric loss values due to substantial space charge polarization caused by accumulation of charges at grain boundaries and defect sites. These charge carriers, which include those associated with oxygen vacancies and dopant-induced defect states, act in accordance with the slowly changing external electric field, leading to increased energy dissipation.

With increasing frequency, these charge carriers' ability to respond to the rapidly alternating field decreases, leading to slow reduction in dielectric loss [30]. Doped samples, particularly Ni- and Co-substituted ZnO, exhibit a higher dielectric loss than pure ZnO due to increased defect density and charge carrier hopping between localized states. If a relaxation peak is observed in the intermediate frequency region, it is associated with a characteristic relaxation process satisfying the condition $\omega\tau \approx 1$ [31]. This indicates non-Debye type relaxation behavior due to the distribution of relaxation times in the heterogeneous system. Thus, the lower dielectric loss at higher frequencies indicates better dielectric stability, making these materials suitable for high-frequency electronic applications.

3.3.3 AC conductivity.

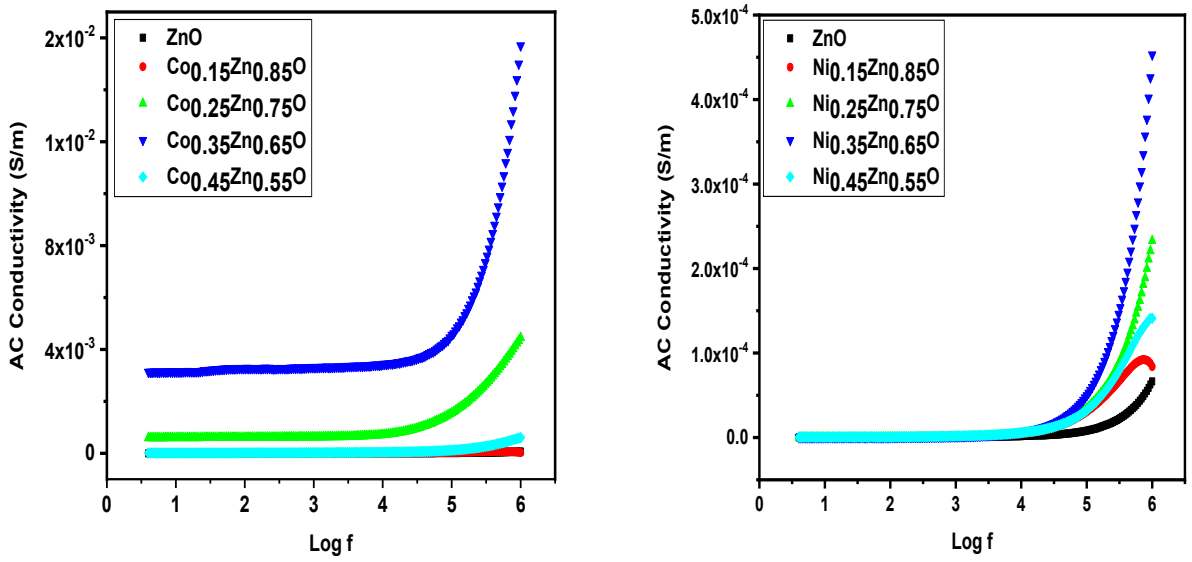

Fig.6. AC conductivity versus frequency of Pure ZnO and Co/Ni doped ZnO Nps.

The AC conductivity (σ_{ac}) of pure and doped ZnO samples has a strong frequency dependence, exhibiting characteristic dispersive behavior that gradually increases with increasing frequency (fig 6). At lower frequencies, conductivity remains relatively low and nearly frequency-independent, indicating the dominance of AC conductivity caused by long-range charge carrier migration limited by grain boundaries. The universal power law signifies frequency-dependent conductivity, indicating a hopping-based conduction mechanism. This behavior indicates that charge transport in these metal oxides is controlled by localized charge carriers that hop between transition metal ion sites.

Among the dopants, Co-doped ZnO has a relatively higher conductivity due to stronger electronic interactions caused by partially filled d-orbitals, which facilitate charge transfer. Furthermore, the observed AC conductivity behavior confirms that these materials' conduction mechanism is dominated by hopping of localized charge carriers, making them suitable for electrical transport properties.

4. Conclusions

The sol-gel auto-combustion process was successfully used to create pristine ZnO, Co-doped, and Ni-doped ZnO NPs with varying concentrations (15%, 25%, 35%, and 45%). Their morphological, structural and electrical characteristics were methodically examined. Following

doping, XRD analysis verified that every sample retained the hexagonal wurtzite structure. However, noticeable lattice distortion was observed for increased Ni doping levels. The appearance of a secondary zinc nickel oxide phase beyond 6% Ni content indicated the solubility limit of Ni in ZnO. The crystallite size decreased with increasing Co doping. For moderate Ni doping (25% and 35%), the crystallite size significantly reduced from 67 nm to 49 nm, accompanied by an increase in lattice strain. SEM analysis revealed agglomerated nanoparticles with mixed morphologies such as spherical, rod-like, and flower-like structures due to Co doping. The particle sizes estimated using ImageJ were consistent with XRD results. SEM also showed a transformation from spherical to polyhedral structures. Ni doping improved particle uniformity and reduced size up to an optimal level, beyond which agglomeration increased. Dielectric studies showed that the dielectric constant and dielectric loss decreased with increasing frequency but increased with higher CO/Ni concentrations. This behavior was explained by the Maxwell–Wagner model of interfacial polarization. Relaxation peaks indicated resonance conditions where charge carriers respond to the applied AC field. AC conductivity increased with frequency, following a hopping conduction mechanism. Ni doping enhanced charge carrier density, improving conductivity at higher frequencies. Overall, Co and Ni doping effectively tuned the structural, dielectric, and electrical properties of ZnO nanoparticles, making them suitable for optoelectronic and high-frequency applications.

References

[1] Keskenler E F, Turgut Gand Dogan S 2012 Investigation of structural and optical properties of ZnO films co-doped with fluorine and indium Superlattices Microstruct. 52107–15.

[2] Biswal R R,V elumani S, Babu B J, Maldonado A,Tirado-Guerra S, Castaneda Lolvera Manddela L 2010 Fluorine doped zinc oxide thin films deposited by chemical spray, starting from zinc pentanedionate and hydrofluoric acid: effect of the aging time of the solution Mater.Sci.Eng.17446–9.

[3] Khan, R., Fashu, S. & Zia-Ur-Rehman Structural, dielectric and magnetic properties of (Al, Ni) co-doped ZnO nanoparticles. *J Mater Sci: Mater Electron* **28**, 4333–4339 (2017). https://doi.org/10.1007/s10854-016-6058-0

[4] Sharma, S., Nanda, K., Kundu, R. S., Punia, R., & Kishore, N. (2015). Structural Properties, Conductivity, Dielectric Studiesand Modulus Formulation of Ni Modified ZnO Nanoparticles. *Journal of Atomic, Molecular, Condensed Matter and Nano Physics*, *2*(1), 15–31. https://doi.org/10.26713/jamcnp.v2i1.307

[5] Sharma, N., Kant, R., Sharma, V. *et al.* Influence of Silver Dopant on Morphological, Dielectric and Magnetic Properties of ZnO Nanoparticles. *J. Electron. Mater.* **47**, 4098–4107 (2018). https://doi.org/10.1007/s11664-018-6305-7.

[6] Belkhaoui, C., Lefi, R., Mzabi, N. *et al.* Synthesis, optical and electrical properties of Mn doped ZnO nanoparticles. *J Mater Sci: Mater Electron* **29**, 7020–7031 (2018). https://doi.org/10.1007/s10854-018-8689-9.

[7] Kant, R., Jakhar, R., & Sharma, A. (2022). Enhanced dielectric and optical performance of (Cu, Ag) co-doped ZnO nanostructures for electronic applications. *Materials Technology*, *37*(13), 2679–2691. https://doi.org/10.1080/10667857.2022.2058835

[8] Kant, R., Sharma, D., Bansal, A., & Singh, R. (2021). Structural, optical and dielectric properties of Al/Mn doped ZnO nanoparticles, a comparative study. *Materials Technology*, *36*(9), 513–520. https://doi.org/10.1080/10667857.2020.1775408.

[9] Imen Ben Elkamel, Nejeh Hamdaoui, Amine Mezni, Ridha Ajjel, Enhancement of dielectric properties of Ni and Co doped ZnO due to the oxygen vacancies for UV photosensors application, Physica E: Low-dimensional Systems and Nanostructures, 119, 2020, 114031, https://doi.org/10.1016/j.physe.2020.114031.

[10] Vegesna, S., Bhat, V.J., Bürger, D. *et al.* Increased static dielectric constant in *ZnMnO* and *ZnCoO* thin films with bound magnetic polarons. *Sci Rep* **10**, 6698 (2020). https://doi.org/10.1038/s41598-020-63195-1.

[11] Muhammad, A., Sajid, M., Khan, M. N., Sheraz, M., Khalid, A., Ahmad, P., Alotibi, S., Al-Saidi, H. M., Sobahi, N., Alam, M. M., Althahban, S.,

Saeedi, A. M., & Albargi, H. B. (2023). Optimization of physical and dielectric properties of Co-doped ZnO nanoparticles for low-frequency devices. *PloS one*, *18*(11), e0287322. https://doi.org/10.1371/journal.pone.0287322.

[12] N. Senthilkumar, I. Vetha Potheher, A. Pramothkumar, M. Meena, R. Mary Jenila, Influence of Co and Ni concentration on the structural, UV transparency and electrical behavior of ZnO nanorod, Materials Science and Engineering: B,302, 2024, https://doi.org/10.1016/j.mseb.2024.117213.

[13] Paskaleva, A., Spassov, D., Blagoev, B., & Terziyska, P. (2024). Peculiarities of Electric and Dielectric Behavior of Ni- or Fe-Doped ZnO Thin Films Deposited by Atomic Layer Deposition. *Materials (Basel, Switzerland)*, *17*(14), 3546. https://doi.org/10.3390/ma17143546.

[14] A. Athira, Bindu P. Nair, A. Chithra Mohan, Beena Saraswathyamma, G. Sivasubramanian, K.M. Sreekanth, K.M. Sreedhar, Electrical behaviour, dielectric properties, then optical behaviour of nickel, magnesium doped/codoped zinc oxide along with preparation, and characterisation, Ceramics International, 51, 9,2025, https://doi.org/10.1016/j.ceramint.2025.01.080.

[15] H. Liu, J. Yang, Z. Hua, Y. Zhang, L. Yang, L. Xiao, Z. Xie, The structure and magnetic properties of Cu-doped ZnO prepared by sol–gel method, Appl. Surf. Sci. 256 (2010) 4162–4165, https://doi.org/10.1016/j.apsusc.2010.01.118.

[16] S. Yun, J. Lee, J. Yang, S. Lim, Hydrothermal synthesis of Al-doped ZnOnanorod arrays on Si substrate, Phys. B 405 (2010) 413–419, https://doi.org/10.1016/j. physb.2009.08.297.

[17] F.A.Akgül, Influence of Ti doping on ZnO nanocomposites: synthesis and structural characterization, Compos. B Eng. 91 (2016) 589–594, https://doi.org/10.1016/j. compositesb.2016.02.015.

[18] H. Jung, D. Kim, H. Kim, The electrical properties of low pressure chemical vapor deposition Ga doped ZnO thin films depending on chemical bonding configuration, Appl. Surf. Sci. 297 (2014) 125–129, https://doi.org/10.1016/j. apsusc.2014.01.096.

[19] A. Abrutis, L. Silimavicius, V. Kubilius, T. Murauskas, Z. Saltyte, V. Plausinaitiene, Doped zinc oxide films grown by hot-wire chemical vapour deposition, Thin Solid Films 276 (2015) 88–97, https://doi.org/10.1016/j.tsf.2015.01.010.

[20] S.K.Krstulovic´, O. Budimlija, J. Kovacˇ, J. Dasovic´, P. Umek, I. Capan, Parameters optimization for synthesis of Al-doped ZnO nanoparticles by laser ablation in water, Appl. Surf. Sci. 440 (2018) 916–925, https://doi.org/10.1016/j. apsusc.2018.01.295.

[21] H. Jung, D. Kim, H. Kim, The electrical properties of low pressure chemical vapor deposition Ga doped ZnO thin films depending on chemical bonding configuration, Appl. Surf. Sci. 297 (2014) 125–129, https://doi.org/10.1016/j. apsusc.2014.01.096.

[22] A. Abrutis, L. Silimavicius, V. Kubilius, T. Murauskas, Z. Saltyte, V. Plausinaitiene, Doped zinc oxide films grown by hot-wire chemical vapour deposition, Thin Solid Films 276 (2015) 88–97, https://doi.org/10.1016/j.tsf.2015.01.010.

[23] Gupta, S.; Tripathi, M. A Review on the Synthesis of TiO2 Nanoparticles by Solution Route. *Open Chem*. **2012**, 10, 279−294.

[24] Kim, S.; Hwang, S.-J.; Choi, W. Visible Light Active Platinum Ion-Doped TiO2 Photocatalyst. *J. Phys. Chem.* B 2005, 109, 24260− 24267.

[25] Lee, M.; Yun, H. J.; Yu, S.; Yi, J. Enhancement in Photocatalytic Oxygen Evolution via Water Oxidation under Visible Light on Nitrogen-Doped TiO2 Nanorods with Dominant Reactive {102} Facets. *Catal. Commun.*2014, 43, 11−15.

[26] Wu, Z.; Dong, F.; Zhao, W.; Wang, H.; Liu, Y.; Guan, B. The Fabrication and Characterization of Novel Carbon Doped TiO2 Nanotubes, Nanowires and Nanorods with High Visible Light Photocatalytic Activity. *Nanotechnol.*2009, 20, 235701.

[27] S. Udaykumar, V. Renuka, J. Chem. Pharmac. Res. 4, 1-6 (2012)

[28] A. Mesaros, C. D. Ghitulica, M. Popa, Synthesis, structural and morphological characteristics,

magnetic and optical properties of Co-doped ZnO nanoparticles. Ceram. Intern. 40, 2835–2846 (2014) https://doi.org/10.1016/j.ceramint.2013.10.030.

[29] Rajendar, V.; Raju, N. Prudhvi; Rao, K. Venkateswara Novel Ammonium Acetate Fuel Based Autocombustion Method for the Preparation of Nickel Doped Zinc Oxide Nanoparticles Advanced Science, Engineering and Medicine, 6, 6, 2014, 683-687.

[30] Muhammad Fawad, Nabeel Maqsood, Ahmad Nawaz, Bilal Islam, Malik Daniyal Zaheer, Kateřina Skotnicová, Synthesis, Characterization, and Enhanced Optical and Dielectric Properties of Pure and Ni-Doped ZnO Nanoparticles for Advanced Electronic Applications, Results in Engineering, 26, 2025, https://doi.org/10.1016/j.rineng.2025.104824.

[31] Elboughdiri N, Iqbal S, Abdullaev S, Aljohani M, Safeen A, Althubeiti K, Khan R. Enhanced electrical and magnetic properties of (Co, Yb) co-doped ZnO memristor for neuromorphic computing. RSC Adv. 2023 Dec 11;13(51):35993-36008. doi: 10.1039/d3ra06853f. Erratum in: RSC Adv. 2025 Mar 24;15(12):8876-8877. doi: 10.1039/d5ra90029h. PMID: 38090095; PMCID: PMC10711987.

*****